DISCOVERY OF SUBSTRUCTURE IN THE SCATTER-BROADENED IMAGE OF SGR A*

C. R. Gwinn[1], Y. Y. Kovalev[2,3], M. D. Johnson[4], and V. A. Soglasnov[2]

[1] Physics Department, Broida Hall, University of California, Santa Barbara, CA 93117, USA; cgwinn@physics.ucsb.edu
[2] Astro Space Center, Lebedev Physical Institute, Russian Academy of Sciences, Profsoyuznaya Str. 84/32, Moscow 117997, Russia
[3] Max Planck Institute for Radio Astronomy, Auf dem Hügel 69, D-53121 Bonn, Germany
[4] Harvard-Smithsonian Center for Astrophysics, 60 Garden Street, Cambridge, MA 02138, USA

ABSTRACT

We have detected substructure within the smooth scattering disk of the celebrated Galactic center radio source Sagittarius A* (Sgr A*). We observed this structure at 1.3 cm wavelength with the Very Long Baseline Array together with the Green Bank Telescope, on baselines of up to 3000 km, long enough to completely resolve the average scattering disk. Such structure is predicted theoretically as a consequence of refraction by large-scale plasma fluctuations in the interstellar medium. Along with the much-studied $\theta_d \propto \lambda^2$ scaling of angular broadening θ_d with observing wavelength λ, our observations indicate that the spectrum of interstellar turbulence is shallow with an inner scale larger than 300 km. The substructure is consistent with an intrinsic size of about 1 mas at 1.3 cm wavelength, as inferred from deconvolution of the average scattering. Further observations of the substructure can set stronger constraints on the properties of scattering material and on the intrinsic size of Sgr A*. These constraints will guide our understanding of the effects of scatter broadening and the emission physics near the black hole in images with the Event Horizon Telescope at millimeter wavelengths.

Key words: black hole physics – Galaxy: nucleus – ISM: structure – radio continuum: ISM – scattering – techniques: interferometic

Online-only material: color figure

1. INTRODUCTION

1.1. Sgr A*

Sgr A* marks a supermassive black hole of mass $4.5 \times 10^6\, M_\odot$ in the center of the Milky Way at a distance of 8.4 kpc (Reid 2009; Ghez et al. 2008). Its close distance and wide spectral range of emission make it an excellent subject for studies attempting to understand the supermassive black holes believed to lie at the core of every galaxy (Richstone 1998; Ho 2008). Sgr A* shows emission in the radio, infrared, and X-ray wavelengths similar to that of the dramatic active nuclei of other galaxies, but with much lower luminosity (Falcke et al. 1998; Genzel et al. 2003; Baganoff et al. 2003; Ghez et al. 2004). Sgr A* appears to be in a relatively quiescent state, raising interesting issues concerning the origin of its emission and its coupling with the surrounding matter. The spectrum, size, and variability are consistent with accretion onto a supermassive black hole (Yuan et al. 2002).

Current radio emission models typically invoke an inefficient accretion flow (Narayan et al. 1995, 1998), a jet (Falcke, & Markoff 2000; Markoff et al. 2007), or a composite (Yuan et al. 2002; Moscibrodzka & Falcke 2013). Pure accretion flow models significantly underpredict the centimeter-wavelength flux from Sgr A* without the addition of a small non-thermal electron population (Mahadevan 1998; Ozel et al. 2000; Yuan et al. 2003). For all models, the intrinsic size increases with wavelength, reflecting the changing location of the photosphere. However, details of the emission morphology are strikingly different—a jet feature will be highly anisotropic, while emission from a non-thermal population may exhibit a limb-brightened shell (Falcke et al. 2000). The intrinsic structure of Sgr A* at centimeter to millimeter wavelengths characterizes regions of the source that are weak or invisible at shorter wavelengths. Hence, measurements of intrinsic size over a broad range of wavelengths are essential for assembling a global picture of accretion and outflow.

1.2. Interstellar Scattering

Perhaps unfortunately, Sgr A* is heavily scattered by interstellar plasma at centimeter and longer wavelengths (Lo et al. 1998; Bower et al. 2006; Lu et al. 2011). The combination of compact emission and heavy scatter broadening at centimeter wavelengths has impeded our understanding of the geometry of Sgr A* and the processes responsible for its emission.

Scattering of radio waves in the interstellar plasma results from small-scale fluctuations in electron density. Evidence suggests that the scatterers are part of a power-law spatial spectrum of density fluctuations (Armstrong et al. 1995). In other words, the difference in electron density between two nearby points has variance that increases as a power law with the separation of the two points. Scattering often displays the Kolmogorov scaling index of $\alpha = 5/3$ expected for a cascade of Alfvén-wave turbulence (Goldreich & Sridhar 1995; Lithwick & Goldreich 2001). The cascade is initiated by driving forces at a large spatial scale, the "outer scale," and is terminated by dissipation at a minimum scale, the "inner scale." The inner scale may be a few hundred kilometers in the interstellar medium (Spangler & Gwinn 1990). The measured $\approx$2:1 anisotropy of the scatter broadening of Sgr A* is typical for heavily scattered lines of sight (Desai & Fey 2001); it may indicate that density fluctuations responsible for scattering are aligned with a large-scale magnetic field (Desai et al. 1994; Goldreich & Sridhar 1995).

A power-law spectrum of turbulence imprints its power-law index on the scattered image. For a scattered point source, it affects the scaling of angular broadening with wavelength and the distribution of flux density with radius (Armstrong et al. 1995). In agreement with the fundamental principle of synthesis

imaging via interferometry, the interferometric visibility as a function of baseline length is the Fourier-conjugate of this distribution, and so the visibility as a function of baseline length reflects the power law with long baselines reflecting small-scale structures. The averaged visibility is expected to be zero for baselines long enough to resolve a smooth scattered image (Gwinn et al. 1998).

1.3. Observations of Scattering of Sgr A*

Very long baseline interferometry (VLBI) observations of Sgr A* reveal a smooth, elliptical-Gaussian image indicative of strong scattering (Krichbaum et al. 1998; Bower et al. 2004; Shen et al. 2005). The image angular size θ scales with observing wavelength λ as λ^2 over a wavelength range of centimeters to a meter (Lo et al. 1985; Jauncey et al. 1989; Krichbaum et al. 1993; Yusef-Zadeh et al. 1994; Shen et al. 2005; Bower et al. 2006; Doeleman et al. 2008; Lu et al. 2011). The smoothness and scaling are consistent with predictions for scattering by density fluctuations in the interstellar plasma, but differ from the scaling of $\theta \propto \lambda^{11/5}$ expected if the fluctuations follow a Kolmogorov spectrum. At shorter wavelengths, the angular size departs from this power law as the source structure becomes important (Doeleman et al. 2008; Lu et al. 2011). By combining observations over a range of wavelengths, observers have inferred a size for the source after deconvolution of the scattering disk to obtain a model-dependent intrinsic size for Sgr A* as a function of wavelength. This deconvolution leads to intrinsic dimensions at 1.3 cm wavelength of about 1 mas, depending on assumptions about the scattering material (Lo et al. 1998; Shen et al. 2005; Bower et al. 2006; Lu et al. 2011).

1.4. Substructure in Scattering Disks

Radio-wave scattering of Sgr A* in the interstellar medium is "strong"; in other words, the multiple paths that the signal takes from source to observer differ in length by many wavelengths. Source images, or interferometric observations, that are subject to strong scattering may be divided into three categories: snapshot, average, and ensemble-average regimes (Narayan & Goodman 1989; Goodman & Narayan 1989). In the "snapshot" regime, phase relationships among paths remain nearly constant during the observation and speckles appear from interference. In the "ensemble-average" limit, an average over many of the possible paths leads to a smooth, stable scattered image. The "average" or "average-image" regime lies between these two; in that regime, averaging has eliminated small-scale variations but left large-scale variations intact. Averaging in time and frequency can shift an observation from the snapshot limit to the average-image regime, as can extended source structure.

For Sgr A*, observations at $\lambda = 1.3$ cm shorter than a few weeks are in the average-image regime because the source is extended. For a single VLBI observation spanning a few hours, substructure in the image should be nearly fixed. Because such structures are smaller than the scattering disk, they modulate the scattered intensity, even on baselines long enough to resolve the average scattering disk. This results in enhanced visibility on long baselines, with a random, noiselike character: it averages out over times longer than that for Galactic rotation to carry the line of sight across the scattered image, or a few weeks. Consequently, theory predicts the rms visibility on long baselines and the average visibility on short baselines (Narayan & Goodman 1989; Goodman & Narayan 1989; Johnson 2013). Recent space VLBI observations using
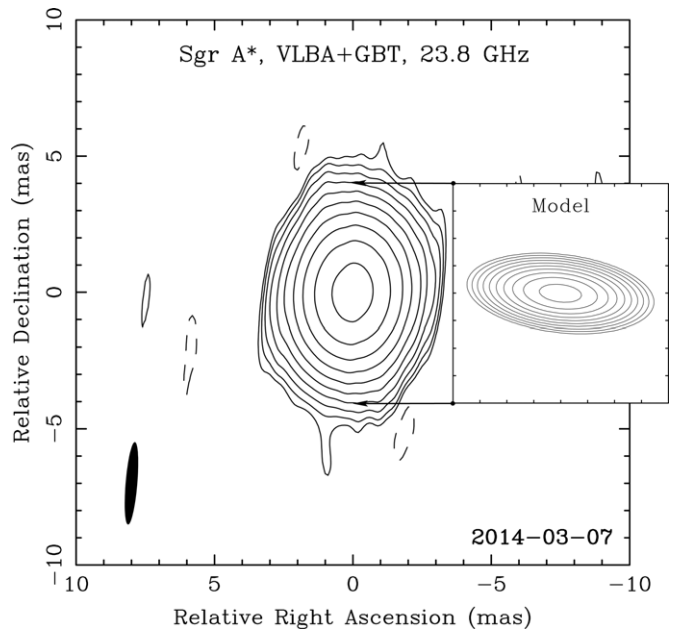

Figure 1. Hybrid image of SgrA* from our naturally weighted data at 1.3 cm showing the scattering disk extended east–west. Substructure would appear as slight variations within the scattering disk. The contours of equal intensity are plotted starting from 0.14% of the peak value of 190 mJy beam^{-1} with $\sqrt{2}$ steps. The restoring beam for the image, shown at lower left, is extended north–south because of the east–west extension of the array which provided detections; the beam has dimensions at half power level (3.04 × 0.42) mas. Nearly all of the north–south extension of the image arises from our elliptical beam. The best-fitting model for the elliptical scattered image is shown as an inset.

the *Radioastron* spacecraft (Kardashev et al. 2013), on baseline projections up to 250,000 km, show such substructure for the heavily scattered Vela pulsar and PSR B0329+54 (C. R. Gwinn et al. in preparation; M. V. Popov et al. in preparation). Moreover, Kellermann et al. (1977) detected strong structure on scales smaller than the scattered image in observations of Sgr A* at $\lambda = 3.6$ cm. Those results suggested the observations reported here.

2. OBSERVATIONS

We observed Sgr A* using the Very Long Baseline Array (VLBA) in concert with the Green Bank Telescope (GBT) at 1.3 cm wavelength on 2014 March 7. For the observations, we used the new NRAO Roach Digital Backend with a digital down-converter and the Mark5C recorder at a bit rate of 2 Gbps. We observed in four contiguous 128 MHz channels with a central frequency of 23.8 GHz, well separated from the H$_2$O line. We recorded left circular polarization with a total bandwidth of 512 MHz and 2 bit sampling. The recent improvements in the recorded bandwidth and the backend have at least doubled the sensitivity of the GBT and VLBA for VLBI observations. The total observing time on Sgr A* was about 3 hr. We also observed the compact extragalactic radio source 1730–130 as a calibration source and obtained strong fringes for it on all baselines.

We performed conventional a priori calibration in AIPS including antenna-based fringe fitting (Greisen 2003), and self-calibration and hybrid imaging in DIFMAP (Shepherd 1997). Figure 1 shows the result. We fitted the size of the scattering disk to our data in the visibility domain using DIFMAP and found a size for the average scattered image of 2.26 × 0.92 mas (FWHM) with the major axis at a position angle of 84°, which
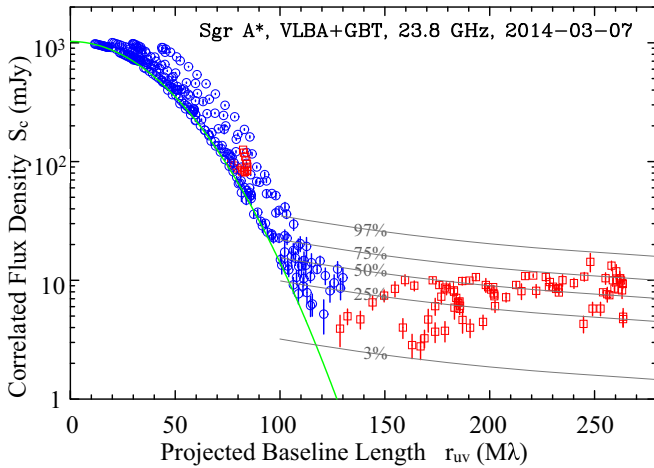
Figure 2. Correlated flux density of Sgr A* at $\lambda = 1.3$ cm plotted against baseline length. Squares show the sensitive GBT–VLBA baselines and circles VLBA–VLBA baselines. Each point represents a 15 minute vector average for one baseline after self-calibration; error bars show statistical $\pm 1\sigma$. The green curve shows the correlated flux density of the average scattering disk for an east–west baseline, as described in Section 2. The gray curves show quantiles of the predicted distribution of correlated flux density from substructure, with source and scattering parameters from Bower et al. (2006, 2014b), as described in Section 3 below.
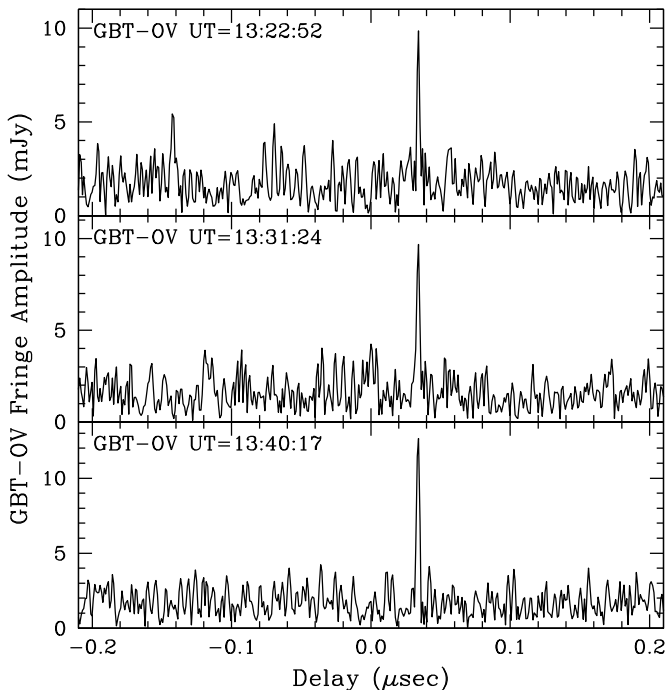

Figure 3. Fringes on Sgr A* on the 3000 km GBT–Owens Valley baseline. To make this plot, we Fourier transformed the data from the correlator, expressed as the complex visibility function as a function of frequency channel and time, to the domain of delay and fringe rate. We located the highest peaks in that domain for each interval and display them here as a function of delay. The average scattering disk has a correlated flux density of $<10^{-6}$ mJy on this baseline. The probability of false detection is $<10^{-9}$ for each of the three peaks.

is consistent with previous results at our observing wavelength (Bower et al. 2004, 2006; Shen et al. 2005; Lu et al. 2011).

Our long GBT–VLBA baselines completely resolve the average scattering disk, but nevertheless revealed a significant excess of correlated flux density (see Figure 2). To verify that these detections are robust, we performed a careful baseline-based fringe search of the data. Figure 3 shows an example: peak correlated flux density for three consecutive 512 s intervals
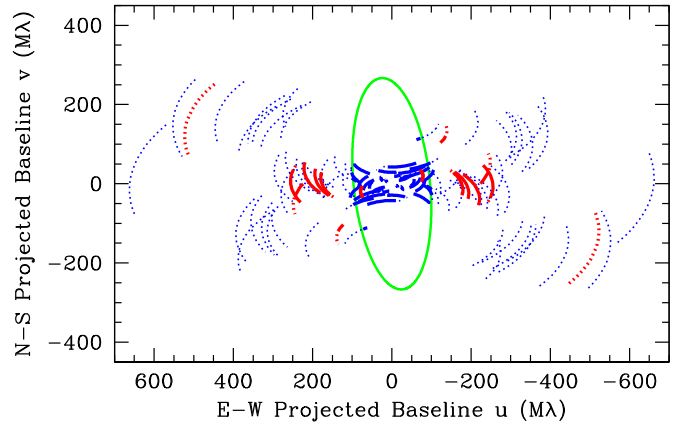

Figure 4. Detections of fringes as a function of position in the plane of baselines perpendicular to the line of sight. GBT–VLBA baselines are shown as red lines and VLBA–VLBA as blue. Detections are solid lines and non-detections are dotted. The green ellipse shows the best-fitting average scattering disk, expressed as the baseline where the correlated flux density reaches $e^{-4} \approx 0.018$ of maximum. Detections on shorter VLBA baselines within the ellipse show the large-scale scattering disk. Detections on long GBT–VLBA baselines indicate substructure within the disk.

for the GBT–Owens Valley baseline. The projected baseline is about 255 Mλ. The peaks range from 8.2 to 10.2 times the rms noise. The probability of attaining such high amplitudes by chance is less than 10^{-9} in any interval (Thompson et al. 2007; Petrov et al. 2011). Moreover, we detect the peak in three consecutive fringing intervals at the same fringe rate and the same delay, and near the values expected from geometric models. We detect the fringes independently in each of the four frequency channels. Results on other long GBT–VLBA baselines with detections were similar to these.

A fit in the visibility domain to a single elliptical Gaussian component, representing only the scattering disk, yielded a reduced $\chi^2 = 1.91$ indicating an unsatisfactory fit. This model could not explain the data at projected spacings longer than 120 Mλ, as shown in Figure 2. Inclusion of a second δ function component to the model with ≈ 10 mJy amplitude yielded a reduced $\chi^2 = 1.28$. Using the method suggested by Kovalev et al. (2005), we found an upper limit to the size of this more compact component of about 0.3 mas in the east–west direction. Thus, analysis by both fringe search and model fitting confirms the presence of highly compact substructure.

We do not believe that the observed fringes could arise from a background source or an intervening source along the line of sight. A background extragalactic source would be scattered as much as Sgr A* or more. A foreground source would have to coincide with Sgr A* to the remarkable angular accuracy demanded by fringe rate and delay. A pulsar with a flux density of 10 mJy at $\lambda = 1.3$ cm would have been detected in previous surveys, and an H_2O maser would be spectrally narrow.

We did not detect fringes on Sgr A* on the GBT–Mauna Kea baseline at a 7σ upper limit of ≈ 5 mJy. The statistics of the visibility were consistent with noise. We were not able to use data from the GBT–Hancock baseline. Saturation or interference effects on this short baseline may have played a role. Sensitivity on baselines to northern antennas in the array, namely, Brewster, Hancock, and the GBT, was significantly reduced due to the low declination of Sgr A*. Figure 4 shows all of our projected baselines, indicating detections.
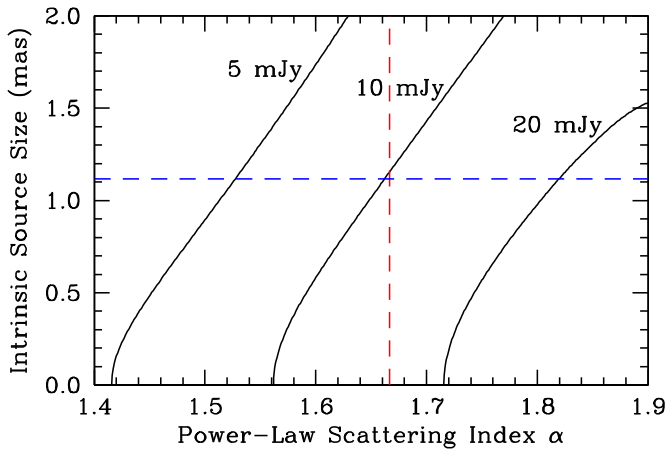
Figure 5. Expected rms level of refractive noise, S_{rms}, on a 3000 km E–W baseline (230 Gλ) as a function of the power-law index of the spectrum of density fluctuations, α, and the intrinsic size (FWHM) of the source θ_{src} along the baseline direction. Each of the three curves is calculated assuming that the diffractive scale and anisotropy are determined by extrapolating longer-wavelength measurements; the scattering geometry determined by Bower et al. (2014a) and Spitler et al. (2014) is assumed. The horizontal dashed line shows the intrinsic size inferred from deconvolution (Bower et al. 2006); the dashed vertical line shows the index α expected for a Kolmogorov spectrum. Samples on other baselines, or at another frequency, would break the degeneracy between α and θ_{src}. Note that because the amplitude of refractive noise is drawn from a Rayleigh distribution, its mean amplitude is $(\sqrt{\pi}/2)S_{rms} \approx 0.89 S_{rms}$ and its median amplitude is $\sqrt{\ln 2} S_{rms} \approx 0.83 S_{rms}$.

(A color version of this figure is available in the online journal.)

3. COMPARISON WITH THEORETICAL MODELS

Although the time and frequency averaging of our data analysis would place us in the snapshot regime for Sgr A*, the source size puts us well into the average-image regime. The large-scale refractive variations left intact in this regime are presumably responsible for the observed substructure in the scattering disk. Such variations would be stochastic with a correlation length (in projected baseline) of approximately the diffractive scale (hundreds of kilometers), they would be broadband, and they would persist over the refractive timescale (weeks). Thus, our current detections sample only a few independent elements of the substructure.

The expected level of refractive substructure depends on the scattering geometry and anisotropy, the spectrum of density fluctuations in the scattering material, and the intrinsic source structure. Because the ensemble-average scattered image depends on these parameters in a different way, our additional measurements can break subtle parameter degeneracies and provide a deeper understanding of the scattering.

Our present measurements set constraints on the spectrum of the density fluctuations that scatters Sgr A*. The observed scaling $\theta \propto \lambda^2$ of image size θ with wavelength λ is consistent with either $\alpha = 2$ or with any "shallow" spectrum ($\alpha < 2$) and an inner scale larger than the diffractive scale: $r_{in} > r_{diff} = 300$ km. Our detection of substructure indicates that the spectrum is shallow with an inner scale larger than the diffractive scale (see Figure 5). A large inner scale increases the level of refractive noise, and so the inner scale cannot substantially exceed the diffractive scale. However, the effect of a large inner scale is slight, scaling the noise by $(r_{in}/r_{diff})^{1-\alpha/2}$. Given the paucity of independent samples in our observations, and the stochastic character of the signal, we can only tentatively conclude that $r_{in} < 10^4$ km. However, additional data that determine the rms

flux density S_{rms} of the stochastic substructure to $\sim$10%, and α from its scaling with baseline, could estimate the inner scale r_{in} to within a factor of two.

Similarly, a small outer scale of the turbulence (relative to the $\sim$3 AU refractive scale) would act to suppress the level of refractive noise (Narayan & Goodman 1989; Goodman & Narayan 1989). Hence, the lack of apparent suppression suggests an outer scale that is at least an AU, as expected from other refractive studies (Armstrong et al. 1995).

Finally, as with other scintillation effects, the substructure is also affected by the source size (Johnson 2013). As a refractive effect, the long baseline noise is quenched for a source that exceeds the refractive scale. The noise is approximately reduced by the squared ratio of the scattered size of a point source to the scattered size of the source. It is important to note that this suppression factor is independent of the baseline length and is only sensitive to the source structure parallel to the baseline. Thus, as with source size estimates via deconvolution, our current measurements are most sensitive to source structure in the east–west direction.

Perhaps the simplest assumption for source and scattering is a point source ($\theta_{src} = 0$) scattered by a Kolmogorov spectrum of turbulence ($\alpha = 5/3$). Under these assumptions, theory predicts a substructure with a rms flux density of $S_{rms} \approx 15$ mJy on our 3000 km baselines. However, by including the 1 mas source size estimated from deconvolution (Bower et al. 2006), we expect $S_{rms} \approx 10$ mJy which is more compatible with our current measurements. This model predicts the distribution of the correlated flux density shown by the gray curves in Figure 2. Figure 5 shows the combinations of α and θ_{src} that are consistent with this level of substructure, and for values of S_{rms} differing by factors of two.

4. SUMMARY

We have detected substructure within the scattered image of Sgr A* at the 1.3 cm wavelength, providing fresh insight into the scattering and structure of this supermassive black hole. Our estimates of source structure at 1.3 cm are complementary to those obtained by deconvolution of the ensemble-average scattering disk, because deconvolution must extrapolate the effects of scattering into ranges of wavelength where they cannot be measured directly. Moreover, our measurements indicate that the turbulent spectrum of the scattering material is shallow, and so the effects of scattering at shorter wavelengths may be *weaker* than previously supposed. We find that the inner scale of that turbulent spectrum is greater than 300 km but less than 10^4 km. We find that the size of the source is consistent with the 1 mas estimates from deconvolution. Additional measurements of substructure over a wider range of baselines and wavelengths can precisely determine the spectrum of density fluctuations and the intrinsic size of Sgr A* at centimeter wavelengths. These will be of critical importance for efforts to image the black hole on event-horizon scales (Doeleman et al. 2008; Fish et al. 2011, 2014).

REFERENCES

Armstrong, J., Rickett, B. J., & Spangler, S. R. 1995, ApJ, 443, 209
Baganoff, F. K., Maeda, Y., Morris, M., et al. 2003, ApJ, 591, 891
Bower, G. C., Deller, A., Demorest, P., et al. 2014a, ApJL, 780, L2
Bower, G. C., Falcke, H., Herrnstein, R. M., et al. 2004, Sci, 304, 704
Bower, G. C., Goss, W. M., Falcke, H., Backer, D. C., & Lithwick, Y. 2006, ApJL, 648, L127
Bower, G. C., Markoff, S., Brunthaler, A., et al. 2014b, ApJ, 790, 1
Desai, K. M., Gwinn, C. R., & Diamond, P. J. 1994, Natur, 372, 754
Doeleman, S. S., Weintroub, J., Rogers, A. E. E., et al. 2008, Natur, 455, 78
Falcke, H., Goss, W. M., Matsuo, H., et al. 1998, ApJ, 499, 731
Falcke, H., & Markoff, S. 2000, A&A, 362, 113
Falcke, H., Melia, F., & Agol, E. 2000, ApJL, 528, L13
Desai, K. M., & Fey, A. L. 2001, ApJS, 133, 395
Fish, V. L., Doeleman, S. S., Beaudoin, C., et al. 2011, ApJL, 727, L36
Fish, V. L., Johnson, M. D., Lu, R.-S., et al. 2014, ApJ, in press (arXiv:1409.4690)
Genzel, R., Schödel, R., Ott, T., et al. 2003, Natur, 425, 934
Ghez, A. M., Salim, S., Weinberg, N. N., et al. 2008, ApJ, 689, 1044
Ghez, A. M., Wright, S. A., Matthews, K., et al. 2004, ApJL, 601, L159
Goldreich, P., & Sridhar, S. 1995, Natur, 438, 763
Goodman, J., & Narayan, R. 1989, MNRAS, 238, 995
Greisen, E. W. 2003, in Information Handling in Astronomy—Historical Vistas, ed. A. Heck (Astrophysics and Space Science Library, Vol. 285; Dordrecht: Kluwer), 109
Gwinn, C. R., Britton, M. C., Reynolds, J. E., et al. 1998, ApJ, 505, 928
Ho, L. C. 2008, ARA&A, 46, 475
Jauncey, D. L., Tzioumis, A. K., Preston, R. A., et al. 1989, AJ, 98, 44
Johnson, M. D. 2013, PhD thesis, Univ. California, Santa Barbara (http://www.cfa.harvard.edu/~mjohnson/Johnson_Dissertation.pdf)
Kardashev, N. S., Khartov, V. V., Abramov, V. V., et al. 2013, ARep, 57, 153
Kellermann, K. I., Shaffer, D. B., Clark, B. G., & Geldzahler, B. J. 1977, ApJL, 214, L61
Kovalev, Y. Y., Kellermann, K. I., Lister, M. L., et al. 2005, AJ, 130, 2473
Krichbaum, T. P., Graham, D. A., Witzel, A., et al. 1998, A&A, 335, L106
Krichbaum, T. P., Zensus, J. A., Witzel, A., et al. 1993, A&A, 274, L37
Lithwick, Y., & Goldreich, P. 2001, ApJ, 562, 279
Lo, K. Y., Backer, D. C., Ekers, R. D., et al. 1985, Natur, 315, 124
Lo, K. Y., Shen, Z.-Q., Zhao, J.-H., & Ho, P. T. P. 1998, ApJL, 508, L61
Lu, R.-S., Krichbaum, T. P., Eckart, A., et al. 2011, A&A, 525, A76
Mahadevan, R. 1998, Natur, 394, 651
Markoff, S., Bower, G. C., & Falcke, H. 2007, MNRAS, 379, 1519
Moscibrodzka, M., & Falcke, H. 2013, A&A, 559, L3
Narayan, R., & Goodman, J. 1989, MNRAS, 238, 963
Narayan, R., Mahadevan, R., Grindlay, J. E., Popham, R. G., & Gammie, C. 1998, ApJ, 492, 554
Narayan, R., Yi, I., & Mahadevan, R. 1995, Natur, 374, 623
Ozel, F., Psaltis, D., & Narayan, R. 2000, ApJ, 541, 234
Petrov, L., Kovalev, Y. Y., Fomalont, E. B., & Gordon, D. 2011, AJ, 142, 35
Reid, M. J. 2009, IJMPD, 18, 889
Richstone, D., Ajhar, E. A., Bender, R., et al. 1998, Natur, 395, A14
Shen, Z.-Q., Lo, K. Y., Liang, M.-C., Ho, P. T.P., & Zhao, J.-H. 2005, Natur, 438, 62
Shepherd, M. C. 1997, in ASP Conf. Ser. 125, Astronomical Data Analysis Software and Systems VI, ed. G. Hunt & H. E. Payne (San Francisco, CA: ASP), 77
Spangler, S., & Gwinn, C. 1990, ApJL, 353, L29
Spitler, L. G., Lee, K. J., Eatough, R. P., et al. 2014, ApJL, 780, L3
Thompson, A. R., Moran, J. M., & Swenson, G. W., Jr. 2007, Interferometry and Synthesis in Radio Astronomy (2nd ed.; New York: Wiley)
Yuan, F., Markoff, S., & Falcke, H. 2002, A&A, 383, 854
Yuan, F., Quataert, E., & Narayan, R. 2003, ApJ, 598, 301
Yusef-Zadeh, F., Cotton, W., Wardle, M., Melia, F., & Roberts, D. A. 1994, ApJL, 434, L63